Electrical conductivity of warm expanded Al

G. Faussurier,[1,*] C. Blancard,[1] P. Renaudin,[1] and P. L. Silvestrelli[2]
[1]*Département de Physique Théorique et Appliquée, CEA/DAM Ile-de-France, Boîte Postale 12-F-91680 Bruyères-le-Châtel, France*
[2]*Dipartimento di Fisica "G. Galilei," Università di Padova, via Marzolo 8, I-35131 Padova, Italy and DEMOCRITOS National Simulation Center, Trieste, Italy*
(Received 12 May 2005; revised manuscript received 13 December 2005; published 8 February 2006)

The electronic and ionic structures of warm expanded aluminum are determined self-consistently using an average-atom formalism based on density-functional theory and Gibbs-Bogolyubov inequality. Ion configurations are generated using a least-squares fit of the pair distribution function deduced from the average-atom model calculations. The electrical conductivity is computed from the Kubo-Greenwood formula for the optical conductivity implemented in a molecular dynamics scheme based on density-functional theory. This method allows us to go beyond the Ziman approach used in the average-atom formalism. Moreover, it is faster than performing quantum molecular dynamics simulations to obtain ion configurations for the conductivity calculation. Numerical results and comparisons with experiments are presented and discussed.

DOI: 10.1103/PhysRevB.73.075106 PACS number(s): 71.30.+h, 72.15.Cz, 52.65.−y

I. INTRODUCTION

The description of matter for the first two decades of decreasing density below solid density and for temperatures from room temperature up to a few electron volts is a very difficult task. In this thermodynamic regime, matter is intermediate between the ordered solid and liquid phases and the highly disordered gas phase. At the present stage, and even for a simple metal as aluminum, experimental data are scarce and there are a very small number of theories that can reproduce thermodynamic data and static transport coefficients of such media in a self-consistent way.[1] This complex thermodynamic equilibrium regime is called the warm dense matter (WDM) regime because it corresponds to the transition between solid-state physics to plasma physics.[2] The WDM regime, which is typically encountered in planetary interiors, in cool dense stars, and in laboratory experiments, opens a challenging field for both experiments and *ab initio* calculations.

At the present time, efficient theoretical approaches to describe the WDM regime are the average-atom and the quantum molecular dynamics approaches. The self-consistent average-atom approach based on finite-temperature density-functional theory[3,4] is a fast method to compute the electronic structure and the pair distribution functions of strongly coupled plasmas of arbitrary degeneracy in local thermodynamic equilibrium (LTE), and obtain that way an equation of state (EOS). It can also be used to estimate the dc conductivity using an extension to finite temperature of the Ziman formula.[5–7] However, multicenter effects are taken into account quite approximatively. Such a method can be unadapted when metal-insulator transition and/or details of the ionic structure play an important role. Moreover, the frequency-dependent part of the conductivity still stays, to our knowledge, hard to calculate, especially when the frequency-dependent real part of the conductivity, i.e., the optical conductivity,[8] shows no Drude character at low frequencies. Such difficulties are not encountered in quantum molecular dynamics (QMD) approach.[9–12] This method incorporates at a high level of accuracy both ionic and electronic structure effects. It treats electron-ion and electron-electron interactions quantum mechanically in the framework of the density-functional theory and makes no *a priori* assumptions about ion-ion forces and the ionic structure. Moreover, the optical conductivity can be computed by means of the Kubo-Greenwood approach.[13–20] The dc conductivity is obtained by extrapolating to zero frequency the ac conductivity. The QMD method is very powerful but has intrinsic limitations, i.e., the pseudopotential assumption and its transferability requirement, the plane-wave expansion with periodic boundary conditions, and the absence of finite-temperature effects in the exchange-correlation functionals currently used. In the same way, we cannot consider very dense situations for which core electrons start to be active. It should be stressed that the general validity of all these assumptions is quite difficult to assess *a priori*. We often need huge capacity memory storage to perform a simulation and to analyze the results. Furthermore, the computation time may be quite large. As a consequence, great care is required to treat high-temperature conditions.

Recently, comparisons with experiments performed in the WDM regime have shown that the average-atom and quantum molecular dynamics approaches can both be used to describe materials in such equilibrium thermodynamic conditions.[4,17–22] Theoretical calculations agree well with experimental data for WDM aluminum, except in the vicinity of a metal/nonmetal transition.[23] In that case, QMD results are in better agreement with measurements than the average-atom calculations. In order to understand these discrepancies, we propose in this paper to face the problematic of calculating the dc conductivity using the Kubo-Greenwood and Ziman formalisms at given pair distribution function. In Sec. II, we propose a method to achieve this task. It reads basically as follows. We use the average-atom model SCAALP (self-consistent approach for astrophysical and laboratory plasmas) to calculate the dc conductivity in the framework of the Ziman formalism. We generate a set of uncorrelated ionic configurations from the pair distribution function obtained with the SCAALP model. This set of ionic configurations is used as an input of the QMD code CPMD (Car-Parrinello

molecular dynamics) to compute the electronic structure without performing any molecular dynamics calculation. The Kubo-Greenwood approach is then used to get the ac conductivity. Finally, we estimate the dc conductivity by extrapolating to zero frequency the optical conductivity. So doing, we keep the strong points of QMD and average-atom approaches while bypassing their weak points. Numerical results and comparisons to measurements are performed and discussed in Sec. III for WDM aluminum. Section IV is the conclusion.

II. METHOD

A. QMD approach

Different QMD approaches have been proposed to describe the properties of condensed matter.[9–11] Here, we use the CPMD method,[24,25] which has been improved by Alavi *et al.*[12] to study the electronic properties of metallic systems at finite temperature. This approach is based on the Mermin density-functional theory.[26] At each QMD step, a self-consistent electronic structure calculation is performed, which takes into account the effect of thermal electronic excitations consistently using fractionally occupied states. The interaction between ions and valence electrons is described using a pseudopotential. For a given configuration of ions $\{R_I\}$ inside a simulation box of volume V_b with periodic boundary conditions, the electronic density $n(\mathbf{r})$ is computed by minimizing the free-energy functional $\mathcal{F}$ of the electron gas. By construction, this functional $\mathcal{F}$ reproduces the exact finite-temperature density of the Mermin functional. $\mathcal{F}$, which is self-consistently optimized for each ionic configuration, reads[17]

$$\mathcal{F} = \Omega + \mu N_e + E_{II}, \tag{1}$$

where

$$\Omega = -\frac{2}{\beta}\ln\det[1+e^{-\beta(\mathcal{H}-\mu)}] - \int d\mathbf{r} n(\mathbf{r})\left[\frac{\Phi(\mathbf{r})}{2}+\frac{\delta\Omega_{xc}}{\delta n(\mathbf{r})}\right]+\Omega_{xc}. \tag{2}$$

The factor two in front of the determinant logarithm stems from considering the spin-unpolarized special case only. $\beta=1/(k_BT)$ with T the electronic temperature and k_B the Boltzmann constant, μ is the chemical potential, and N_e is the total number of valence electrons. $\mathcal{H}=-\hbar^2\nabla^2/(2m)+V(\mathbf{r})$ is the one electron Hamiltonian associated to the effective potential $V(\mathbf{r})=\Sigma_i e^2Z_i/|\mathbf{r}-\mathbf{R}_i|+\Phi(\mathbf{r})+\delta\Omega_{xc}/\delta n(\mathbf{r})$, where $\hbar$ is the reduced Planck constant, m and e are the electronic mass and charge, and Z_i is the charge of ion i. $\Phi(\mathbf{r})=e^2\int d\mathbf{r}' n(\mathbf{r}')/|\mathbf{r}-\mathbf{r}'|$ and Ω_{xc} are the Hartree potential energy of an electron gas of density $n(\mathbf{r})$ and the exchange-correlation energy in the local-density approximation (LDA), respectively. Finally, $E_{II}=\Sigma_{i<j}e^2Z_iZ_j/|\mathbf{R}_i-\mathbf{R}_j|$ is the classical Coulomb energy of the ions. The exchange-correlation functional Ω_{xc} is approximated by its zero-temperature expression.[12,17] Thermodynamic equilibrium between electrons and ions is assumed in the simulations, so that the electronic temperature is equal to the average ionic temperature. The one-electron Hamiltonian is diagonalized by means of an efficient variant of the Lanczos algorithm. The electronic density is expressed in terms of single-particle orbitals Ψ_k

$$n(\mathbf{r}) = \sum_k \frac{|\Psi_k(\mathbf{r})|^2}{1+e^{\beta(E_k-\mu)}}. \tag{3}$$

The chemical potential is adjusted such that $\int d\mathbf{r} n(\mathbf{r})=N_e$. The electronic orbitals Ψ_k are the one-electron eigenstates of $\mathcal{H}$ with eigenvalues E_k

$$\mathcal{H}\Psi_k(\mathbf{r}) = E_k\Psi_k(\mathbf{r}). \tag{4}$$

$\mathcal{H}$ is evaluated with $n(\mathbf{r})$ in this set of equations of the Kohn-Sham form. The ionic forces are calculated using the Hellmann-Feynman theorem. The overall procedure ensures a self-consistent calculation of electronic and ionic structures. Once the thermalization is achieved one can select a set of uncorrelated QMD configurations on the fly as the simulation proceeds, and obtain that way, for instance, a configuration-average optical electronic conductivity $\sigma(\omega)$ by means of the Kubo-Greenwood formula.[17] In this approach, $\sigma(\omega)$ is computed as a configurational average of

$$\sigma(\omega) = \frac{2\pi e^2}{3m^2\omega}\frac{1}{V_b}\sum_{k,k'}(f_k-f_{k'})|<\Psi_k|\hat{p}|\Psi_{k'}>|^2 \times \delta(E_{k'}-E_k-\hbar\omega), \tag{5}$$

where $\hat{p}$ is the momentum operator and Ψ_k, E_k, are the electronic density-functional theory (DFT) eigenstates and eigenvalues, calculated for the ionic configuration $\{R_I\}$, at the single k point (for instance, the Γ point) of Brillouin zone. The generalization of Eq. (5) to more than one k-vector sampling is straightforward

$$\sigma(\omega) = \sum_{\mathbf{k}} \sigma(\omega,\mathbf{k})W(\mathbf{k}), \tag{6}$$

where $\sigma(\omega,\mathbf{k})$ is defined by Eq. (5), with the eigenstates and the eigenvalues computed at $\mathbf{k}$, and $W(\mathbf{k})$ is the weight of the point $\mathbf{k}$. Of course, the use of the single-particle DFT-LDA states and eigenstates, instead of the true many-body eigenfunctions and eigenvalues, introduces an approximation in the calculation of the electrical conductivity. Note also that the procedure of calculating the optical electronic conductivity by averaging over selected arrangements of atoms, and obtain that way results representative of the finite-temperature sample, induces an approximative treatment of the electron-phonon interaction. This "snapshot" treatment of the electron-phonon interaction makes sense at relatively high temperatures compared to the Debye temperature. This was the case in Ref. 17 and for the thermodynamic situations encountered in the present work. Due to finite-size discretization of the eigenvalues spectrum, $\sigma(\omega)$ is computed for a finite set of frequencies $(\omega_1,\omega_2,\ldots,\omega_l,\ldots)$ by averaging over a small frequency range $\Delta\omega$

$$\sigma(\omega_l) \approx \frac{1}{\Delta\omega}\int_{\hbar\omega_l-\Delta\omega/2}^{\hbar\omega_l+\Delta\omega/2} \sigma(\omega)d\omega. \quad (7)$$

The value of $\Delta\omega$ has to be large enough to ensure that a sufficient number of electronic levels contribute, and, at the same time, small enough to allow a good resolution. We stress that such a quantum statistical-mechanics determination of electrical conductivity has been successfully performed by studying various systems including liquids and dense plasmas. The agreement with the experimental results turned out to be generally satisfactory.[17–22,27,28]

B. Average-atom approach

Many attempts have been made to obtain an average-atom model from first principles to describe the statistical properties and the transport coefficients of strongly coupled plasmas of arbitrary degeneracy in LTE. Here, we consider the SCAALP model based on the neutral pseudoatom (NPA) concept.[4] At given temperature T and mass density ρ, the plasma is represented as an effective classical system of virtual neutral particles, i.e., a collection of NPA's interacting via an interatomic effective pair potential Φ

$$\Phi(\mathbf{R}) = 2E_X(\mathbf{R}) - Zv_{at}(\mathbf{R}) + \int \rho_e(\mathbf{r})v_{at}(\mathbf{r}-\mathbf{R})d\mathbf{r}, \quad (8)$$

where $v_{at}(\mathbf{r}) = -Ze^2/|\mathbf{r}| + \int e^2\rho_e(\mathbf{r}')/|\mathbf{r}-\mathbf{r}'|\,d\mathbf{r}'$, Z is the nuclear charge, $\rho_e(\mathbf{r})$ is the NPA electronic density, and $E_X(\mathbf{R})$ is the exchange energy coming from two groups of electrons belonging to different ions, one placed at the origin and the other at $\mathbf{R}$. The whole NPA's are assumed to have the same electronic density $\rho_e(\mathbf{r})$ and the same set of one-electron orbitals $\varphi_n(\mathbf{r})$ and energies ε_n. These $\varphi_n(\mathbf{r})$ and ε_n are solutions of a Schrödinger equation with a central symmetric effective potential $v_{\text{eff}}(\mathbf{r})$

$$\left[-\frac{\hbar^2\nabla^2}{2m} + v_{\text{eff}}(\mathbf{r})\right]\varphi_n(\mathbf{r}) = \varepsilon_n\varphi_n(\mathbf{r}). \quad (9)$$

The NPA electronic density $\rho_e(\mathbf{r})$ is equal to

$$\rho_e(\mathbf{r}) = \sum_n \frac{|\varphi_n(\mathbf{r})|^2}{1+e^{\beta(\varepsilon_n-\mu)}} \quad (10)$$

with

$$\int \rho_e(\mathbf{r})d\mathbf{r} = Z \quad (11)$$

to ensure charge conservation. This is accomplished by adjusting the electronic chemical potential μ. The integration is performed over the entire Wigner-Seitz cell of radius R_{WS}, with one NPA placed at the origin of coordinates. Introducing the ion density $\rho_i = \rho\mathcal{N}/A$, where $\mathcal{N}$ and A are the Avogadro constant and the molar mass, respectively, the Wigner-Seitz radius R_{WS} is such that $4\pi R_{\text{WS}}^3\rho_i/3 = 1$. The v_{eff} expression is established by using a variational principle based on the Gibbs-Bogolyubov inequality. In this way, we find the best one-electron trial Hamiltonian $\mathcal{H}_0 = -\hbar^2\nabla^2/(2m) + v_{\text{eff}}(\mathbf{r})$, in the sense of the Gibbs-Bogolyubov inequality, i.e., the best NPA one-electron density $\rho_e(\mathbf{r})$, to represent the original many-body Hamiltonian of the overall electron and bare nucleus neutral system. In the same spirit, we use an hard-sphere (HS) reference system with an effective packing-fraction η to represent the collection of NPA's interacting via the effective pair potential Φ. We can thus calculate the free energy per NPA associated with Φ in the sense of the Gibbs-Bogolyubov inequality, i.e., by determining the best HS packing fraction to represent the original effective classical system of NPA's. This is done by minimizing the total free energy per NPA F_{tot} of the system with respect to both the NPA electronic density $\rho_e(\mathbf{r})$ and the effective HS packing-fraction η. The expression for F_{tot} reads as follows:

$$F_{\text{tot}} = F_I^{\text{id}} + F_{\text{HS}}^{\text{ex}}(\eta) + \frac{\rho_i}{2}\int g_{HS}(\eta,\mathbf{R})\Phi(\mathbf{R})d\mathbf{R} + F_e, \quad (12)$$

where F_I^{id} is the ideal free energy of a perfect gas, $F_{\text{HS}}^{\text{ex}}(\eta)$ and $g_{\text{HS}}(\eta,\mathbf{R})$ are the excess free energy, and the pair distribution function of the HS reference system, and F_e the free energy electronic contribution

$$F_e = -\frac{1}{\beta}\sum_n \ln[1+e^{-\beta(\varepsilon_n-\mu)}] + E_X(0) - \frac{e^2}{2}\int\int \frac{\rho_e(\mathbf{r})\rho_e(\mathbf{r}')}{|\mathbf{r}-\mathbf{r}'|}d\mathbf{r}d\mathbf{r}' + \int \rho_e(\mathbf{r})v_{at}(\mathbf{r})d\mathbf{r} - \int \rho_e(\mathbf{r})v_{\text{eff}}(\mathbf{r})d\mathbf{r} + Z\mu. \quad (13)$$

In practice, we consider the spin-unpolarized special case only. The whole quantities F_I^{id}, $F_{\text{HS}}^{\text{ex}}(\eta)$, and F_e are understood to be per NPA. F_I^{id} is well-known.[29] We use the Carnahan-Starling expression for $F_{\text{HS}}^{\text{ex}}(\eta)$ and $g_{\text{HS}}(\eta,\mathbf{R})$ is calculated using the Percus-Yevick approximation.[30] The Gibbs-Bogolyubov inequality (GBI) for ions (electrons) states that F_{tot} is minimum for any variation of η (ρ_e) at fixed T, ρ_i, Z, and ρ_e (η), i.e.,

$$\frac{\partial F_{\text{tot}}}{\partial\eta} = 0 \quad (14)$$

leads to

$$\frac{\rho_i}{2}\int \frac{\partial g_{\text{HS}}(\eta_{\text{eff}},\mathbf{R})}{\partial\eta}\Phi(\mathbf{R})d\mathbf{R} = 0, \quad (15)$$

whereas

$$\frac{\delta F_{\text{tot}}}{\delta\rho_e(\mathbf{r})} = 0 \quad (16)$$

leads to

$$v_{\text{eff}}(\mathbf{r}) = v_{at}(\mathbf{r}) + \frac{\delta E_X(0)}{\delta \rho_e(\mathbf{r})} + \rho_i \int \left[v_{at}(\mathbf{r}-\mathbf{R}) + \frac{\delta E_X(\mathbf{R})}{\delta \rho_e(\mathbf{r})} \right] g_{\text{HS}}(\eta, \mathbf{R}) d\mathbf{R}. \quad (17)$$

Equations (15) and (17) determine the effective HS packing-fraction η_{eff} and the effective electron-ion potential v_{eff}, respectively. In Eqs. (17), the electrostatic part results in a simple charge superposition. This means that to calculate the electrostatic potential at a given radius, we only need to add the electrostatic potential of the NPA located at the origin and the electrostatic potential of the other NPA of the plasma, with the conditional probability that there is a NPA at the origin, hence the presence of the pair distribution function $g_{\text{HS}}(\eta, \mathbf{R})$. The exchange contribution is more complicated to interpret, except if we consider the density-functional theory in the local-density approximation, where a similar conclusion may be drawn using the exchange potential. In practical calculations, the DFT in LDA is used to estimate the exchange and correlation effects for the model to be computationally tractable. As for electrons, we have adopted the numerical schemes of the DFT in the LDA proposed by Iyetomi and Ichimaru[31] at finite temperature, after intensive comparisons with experiments.[4] As for consistency, we have kept the same approach for ions using the Gordon and Kim[32] method to estimate the exchange contribution within the effective ionic pair potential. Knowledge of the total free energy of the plasma gives access to the main thermodynamic quantities of interest by numerical differentiation. Finally, we employ the Ziman formalism to calculate the dc electrical conductivity of the system from the inverse of the electrical resistivity ϱ given by[33]

$$\varrho = -\frac{\hbar}{3\pi \bar{Z}^2 e^2 \rho_i} \int_0^\infty d\varepsilon f'(\varepsilon) \int_0^{2k} dq q^3 S(q) \sigma_{\text{sc}}(q), \quad (18)$$

where $q^2 = 2k^2(1-\cos\theta)$. Here $\mathbf{q}$ is the momentum transferred from the incident electron with energy $\varepsilon = \hbar^2 k^2/(2m)$. The derivative of the Fermi-Dirac distribution for the electrons $f(\varepsilon) = 1/[1+e^{\beta(\varepsilon-\mu)}]$ is denoted by $f'(\varepsilon)$. The structure factor $S(q)$ of the ion distribution is calculated using the Percus-Yevick approximation for the HS system with packing-fraction η_{eff}. The differential scattering cross section $\sigma_{\text{sc}}(q)$ depends on the incident-electron momentum $\mathbf{k}$ and the transferred momentum $\mathbf{q}$. $\sigma_{\text{sc}}(q)$ is obtained from the phase shifts of v_{at}. Finally, the effective average ionization $\bar{Z}$ is given by $\bar{Z} = \rho_e(R_{WS})/\rho_i$.[34] In practical applications of the Ziman formula, various approximations are currently made.[7] Here, the Ziman formula is employed in consistency with the average-atom model used to calculate equation of state (EOS) data.

C. Combination of QMD and average-atom approaches

In practical applications, these two *ab initio* approaches are used independently to calculate EOS and electrical conductivity of materials in LTE. In order to test their domain of validity, it is interesting to extend QMD calculations from solid density and room temperature to temperatures of a few electron volts and densities equal to some fractions of solid density, whereas average-atom calculations can be pushed from hot dense plasma conditions to temperatures down to 1 eV and to some fractions of solid density. Clearly, there is a thermodynamic regime, i.e., the WDM regime, where QMD and average-atom approaches can be compared to each other. Moreover, the WDM appears to be also a thermodynamic domain inside which the two methods are both questionable. Recent comparisons with experimental results for WDM aluminum[4,17–22] have shown that the QMD and average-atom calculations are close to each other. They agree well with experimental data except near a metal/non-metal transition,[23] where a better agreement with measurements has been observed with the QMD calculations. In order to understand this fact, we propose to calculate the dc conductivity using the Kubo-Greenwood and Ziman formalisms at fixed pair distribution function. The general methodology works as follows. We calculate the electronic structure and the radial pair distribution function $g_{\text{HS}}(\eta, R)$ in a self-consistent way with the SCAALP code for one element in LTE conditions at given T and ρ. We distribute randomly N_a ions in a simple cubic unit cell $\mathcal{C}$ of length c with periodic boundary conditions such that $\rho_i = N_a/V_b$ with $V_b = c^3$. The $3N_a$ unknown ion coordinates inside the cubic cell $\mathcal{C}$ are determined by fitting the pair distribution function $g_{\mathcal{C}}(R)$ calculated inside the cubic cell[35] to the known pair distribution function $g_{\text{HS}}(\eta, R)$. The minimum image convention is adopted. We limit the calculation of $g_{\mathcal{C}}(R)$ and $g_{\text{HS}}(\eta, R)$ to distances less than half the box-length. We use the Powell method[36] to minimize χ

$$\chi = \sum_{i<j} |g_{\text{HS}}(\eta, R_{ij}) - g_{\mathcal{C}}(R_{ij})|^2, \quad (19)$$

where R_{ij} is the minimum image separations of all the pairs of ions $\{ij\}$.[35] We generate as many uncorrelated ionic configurations as we need, starting the minimization process with randomly located ions inside the cubic cell $\mathcal{C}$. Once selected that way a set of ionic configurations, we calculate the electronic structure for each ionic configuration with the CPMD code. We then estimate the optical conductivity using the Kubo-Greenwood formula with the CPMD code by averaging over the ionic configurations. This method is adapted to thermodynamic conditions and materials for which the pseudopotential and exchange-correlation functional used in the CPMD code make sense.

III. NUMERICAL APPLICATIONS

In this section, our method is tested by performing comparisons with experimental results and theoretical calculations for aluminum in the WDM regime. We have chosen aluminum because this element is widely used in technical applications and its properties, particularly conductivity, are of considerable importance. Our main interest concerns the improvement brought about by using the CPMD code as a postprocessor of the SCAALP model to compute the conductivity with the Kubo-Greenwood formula over the simple Ziman approach. We call this method SCAALP-CPMD.

The whole calculations with the CPMD code have been performed, at constant volume, in a periodically repeated simple cubic box or supercell containing N_a aluminum atoms dispatched as explained in the previous section. The interaction between ions and valence electrons has been modeled using a norm-conserving pseudopotential with s and p nonlocality.[37] The electronic orbitals were expanded in plane waves with a cutoff of 16 Ry. This aluminum pseudopotential has been carefully tested and successfully used in QMD simulations of solid and molten aluminum at the melting point[38] and to study metal-insulator transition in dense aluminum.[17] Since the CPMD code has been used successfully for aluminum from liquid-metal conditions to WDM regime,[17] we have kept the same CPMD parameters to consider here more expanded and hotter aluminum WDM. We generate ten uncorrelated ionic configurations using the pair distribution function of the SCAALP model. For each ionic configuration, the electronic conductivity is computed by means of the Kubo-Greenwood approach, once achieved the self-consistent field calculation of the electronic excitation spectrum using the Γ point to sample the Brillouin zone. In the density and temperature ranges covered in this work, i.e., ρ between 0.01 and 1.0 g/cm^3 and T between 10 000 to 35 000 K, it has been shown that even at low densities, the results are fortunately not sensitive to the choice of $\mathbf{k}$ points.[18] This explains why we use only the Γ point, which, through the symmetry, significantly reduces the computational effort. Due to finite-size discretization of eigenvalue spectrum (N_s excited states, depending on T, ρ, and N_a), the optical conductivity is averaged over a small frequency range $\Delta\omega=0.2$ eV.[17] The dc conductivity is obtained by extrapolating to zero frequency this coarse-grained optical conductivity using a cubic regression on the points between 0.1 and 1.1 eV for ρ between 0.1 and 1.0 g/cm^3, and between 0.1 and 3.3 eV for $\rho=0.01$, 0.025, and 0.05 g/cm^3. The regression is performed keeping the cloud of values of the ten statistically independent ionic configurations, instead of averaging the ac conductivity over the ensemble of ionic configurations sampled first, and doing the regression over this averaged ac conductivity afterward. This sounds physically wiser, especially when fluctuations of the ac conductivity near zero frequency are present.

As a first example, we have considered an aluminum isotherm at $T=10\,000$ K for densities between 0.001 and 1.0 g/cm^3. The parameters of the CPMD calculations and the effective HS packing-fraction η_{eff} predicted by the SCAALP model can be found in Table I. In Fig. 1,we compare the dc conductivity obtained by the SCAALP model,[23] by the SCAALP-CPMD approach, and by the calculations done by Desjarlais *et al.*[18] using the quantum molecular dynamics code VASP (Ref. 11) (Vienna ab initio simulation program) with measurements using exploded wires. The corresponding data have been extracted from Refs. 39 and 40. We have also included experimental data points obtained using aluminum foil strips tamped by polished glass plates and rapidly heated by means of a pulse current.[41] Concerning the latter, we have chosen the closest temperatures to 10 000 K because we do not have values for $T=10\,000$ K in Ref. 41: $T=9361.54$ and 10 660.89 K for $\rho=1.0$ g/cm^3, $T=9967.88$ K for $\rho=0.675$ g/cm^3,

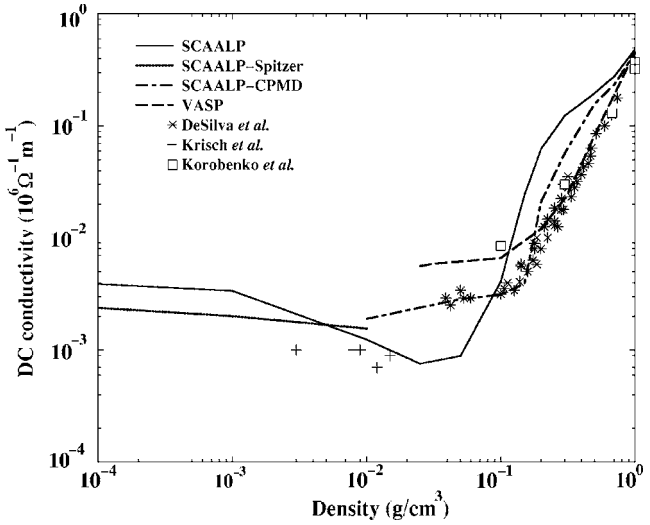

FIG. 1. DC conductivity of aluminum at $T=10\,000$ K as a function of density obtained by the SCAALP model (SCAALP) (Ref. 4), by using the SCAALP model with the Spitzer formula (Ref. 42) (SCAALP-Spitzer), by combining the SCAALP and the CPMD (Ref. 17) models (SCAALP-CPMD), and by the VASP code (VASP) (Ref. 18) compared to experimental results obtained using exploded wires [DeSilva and Katsouros (Ref. 39) and Krisch and Kunze (Ref. 40)] and using pulse current [Korobenko *et al.* (Ref. 41)].

$T=10\,292.95$ K for $\rho=0.3$ g/cm^3, and $T=10\,220.59$ K for $\rho=0.1$ g/cm^3. To be complete, it can be noticed that contrary to the experiments described in Refs. 39 and 41, Krisch and Kunze[40] were able to determine the plasma parameters density and temperature independently, so that no EOS model is needed to infer the experimental data. At low density, we have also included the Spitzer formula[42] using the average ionization of the SCAALP model (SCAALP-Spitzer). As for SCAALP-CPMD, we have tried, as far as we can, to consider the largest number N_a of ions per supercell $\mathcal{C}$ to improve the statistics, i.e., $N_a=108$. This is possible for densities from 1.0 g/cm^3 down to 0.2 g/cm^3. For 0.1, 0.05, 0.025, and 0.01 g/cm^3, we took fewer ions inside $\mathcal{C}$ for computational limitation, i.e., $N_a=64$, 32, 16, and 8, respectively. This number of atoms per supercell is still larger than or at least equal to the value $N_a=32$ used in previous QMD simulations with the VASP code for densities from 0.05 g/cm^3 up to 1.0 g/cm^3.[18,20] The agreement between experimental and theoretical results is good, even for the SCAALP model based on the Ziman formula. The SCAALP-CPMD method is better that the SCAALP model everywhere. Note that at low densities, the SCAALP model underestimates the dc conductivity measurements compared to the SCAALP-CPMD method, whereas the opposite trend is observed at intermediate densities. The discrepancy between the SCAALP and the SCAALP-CPMD results between 0.1 and 1.0 g/cm^3 can be explained by a significant degree of electronic charge localization, which can be understood by assuming the localization of the atomic $3s$ and $3p$ orbitals.[22] Indeed, SCAALP calculations indicate that the $3s$ orbital is bound at 0.5 g/cm^3 and below but not at 0.7 and 1.0 g/cm^3, whereas the $3p$ orbital is bound at 0.1 g/cm^3 and below but not between 0.2 and 1.0 g/cm^3. Below 0.1 g/cm^3, the dis-

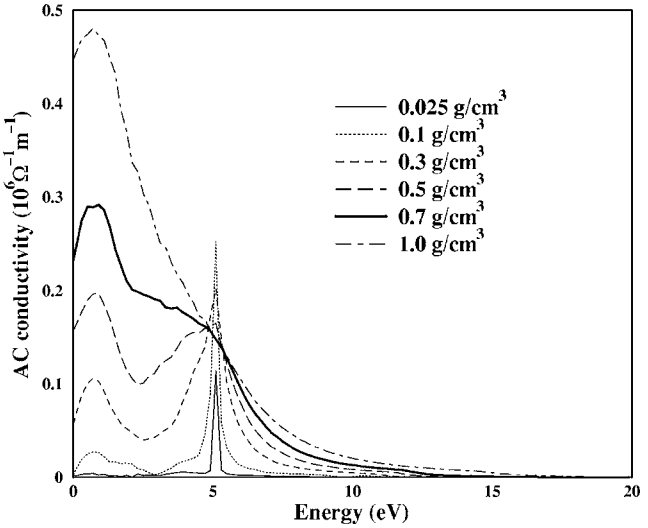

FIG. 2. AC conductivity of aluminum at $T=10\,000$ K and $\rho=0.025$, 0.1, 0.3, 0.5, 0.7, and 1 g/cm^3 obtained by combining the SCAALP (Ref. 4) and the CPMD (Ref. 17) models.

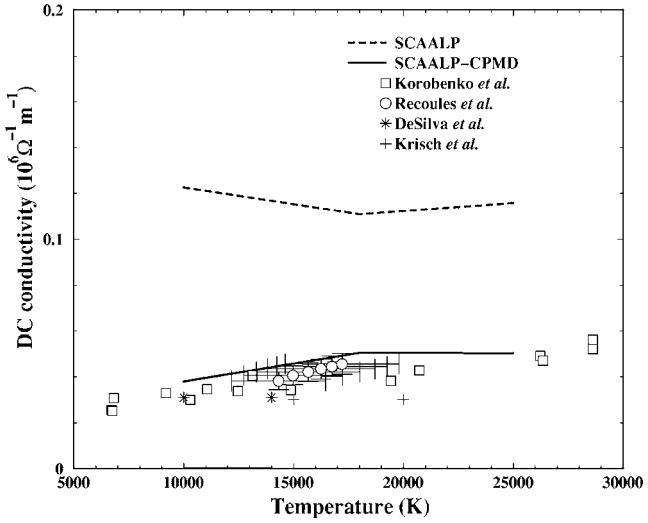

FIG. 3. DC conductivity of aluminum at $\rho=0.3$ g/cm^3 as a function of temperature obtained by the SCAALP model (SCAALP) (Ref. 4) and by combining the SCAALP and the CPMD (Ref. 17) models (SCAALP-CPMD) compared to experimental results obtained using exploded wires [DeSilva and Katsouros (Ref. 39) and Krisch and Kunze (Ref. 40)], using pulse current [Korobenko *et al.* (Ref. 41)], and with isochoric plasma closed vessel [Recoules *et al.* (Ref. 19)].

crepancy between the SCAALP and the SCAALP-CPMD results can be attributed to the treatment of neutral species.[22] The SCAALP calculations show that the average ionization $\bar{Z}$ is smaller than 0.1 in this density range. Since the Ziman formula for the electrical resistivity is proportional to the $1/\bar{Z}^2$, any uncertainty in the $\bar{Z}$ calculation may have a strong impact on the electrical resistivity value. This is particularly true when neutral species dominate, i.e., when $\bar{Z}$ becomes very small. Now, let us compare the SCAALP-CPMD and the VASP calculations to experiment. In Fig. 1, we see clearly that the VASP results are closer to measurements than the SCAALP-CPMD results between 0.1 and 1.0 g/cm^3. At low densities, we observe an interesting trend. There is a discrepancy between the experimental data obtained from the exploded wires and pulse current techniques. Indeed, the VASP results agree with the pulse current data,[41] whereas the SCAALP-CPMD results are closer to the exploded wires data.[39,40] To our knowledge, no quantum molecular dynamics calculations are yet available for densities lower than 0.01 g/cm^3 for aluminum at $T=10\,000$ K to compare to the data of Krisch and Kunze.[40] It is rather difficult to understand the various trends of the experimental data observed in Fig. 1 around 0.1 g/cm^3 and at lower densities. A possible explanation can be proposed by remembering that in Refs. 39 and 41, the SESAME EOS tables[43] are employed to determine the plasma parameters density and temperature instead of measuring them, as done in Ref. 40. Determining both the plasma parameters density and temperature from standard EOS tables instead of measuring them may be questionable, especially for aluminum when $0.1<\rho<2$ g/cm^3 and $1<T<50$ eV.[44] In summary, the best agreement with the measurements between 1.0 and 0.2 g/cm^3 is obtained with the VASP calculations results. Experimental data points obtained without using any EOS model should be welcome to span continuously the transitional density range around 0.1 g/cm^3 down to 0.001 g/cm^3. The SCAALP model is the only approach that can be compared to experimental results by going from high densities, for which the dc conductivity can be described by the Ziman formula, to low densities, for which the dc conductivity approaches the Spitzer values, and passing through a minimum around 0.05 g/cm^3. The overall agreement of the SCAALP-CPMD results with experiment was not evident *a priori* due to the dramatic change of the optical conductivity over the density range shown in Fig. 1.

As an illustration, we plot the aluminum optical conductivity at $T=10\,000$ K in Fig. 2 for $\rho=0.025$, 0.1, 0.3, 0.5, 0.7, and 1 g/cm^3, respectively. At solid density, the optical conductivity is known to be almost indistiguishable from a Drude form, indicating the nearly free-electron nature of the system.[8] For a range of intermediate densities, i.e., between 1.0 and 0.5 g/cm^3, the low frequency part of the optical conductivity shows no Drude character. As quoted in Ref.

TABLE I. Parameters of the CPMD and SCAALP calculations for aluminum at $T=10\,000$ K. ρ, N_a, N_s, and η_{eff} are the mass density, the number of ions in the cubic supercell $\mathcal{C}$, the number of excited states, and the effective HS packing fraction, respectively.

ρ (g/cm^3)	N_a	N_s	η_{eff}
0.01	8	1800	0.013
0.025	16	1800	0.012
0.05	32	1800	0.022
0.1	64	2000	0.046
0.2	108	2000	0.078
0.3	108	1600	0.091
0.5	108	1200	0.104
0.7	108	1000	0.114
1.0	108	1000	0.127

TABLE II. Parameters of the CPMD and SCAALP calculations for aluminum at $\rho=0.3$ g/cm^3. T, N_a, N_s, and η_{eff} are the temperature in kelvin, the number of ions in the cubic supercell $\mathcal{C}$, the number of excited states, and the effective HS packing fraction, respectively.

T (K)	N_a	N_s	η_{eff}
10 000	32	800	0.091
18 000	32	1200	0.087
25 000	32	1840	0.084

18, a pseudogap is just beginning to form at the Fermi energy with lowering density producing an optical conductivity peak located between 4 and 6 eV. At lower densities, the amplitude of the peak becomes prominent near 5.1 eV, compared to the optical conductivity near zero energy. This peak is interpreted as a $3s \rightarrow 3p$ transition. Its energy is close to the $3s \rightarrow 3p$ transition for an isolated atom.[45] The SCAALP-CPMD results are consistent with the calculations obtained by Desjarlais *et al.*[18]using complete QMD simulations. This interpretation is corroborated by the energy estimation of the $3s \rightarrow 3p$ transition using the one-electron energies predicted by the SCAALP model: 4.9 eV at 0.1 g/cm^3 and 5.0 eV at 0.025 g/cm^3. Combining a plasma physics model, i.e., SCAALP, with QMD approach, CPMD, confirms that a condensed matter approach can represent the basic characteristics of a diffuse plasma. Moreover, it gives another strong indication that high-temperature plasma physics models and low-temperature condensed-matter methods can merge smoothly in the WDM regime and can be used quite safely in conjunction.[22,23]

These comparisons with experimental data show that the SCAALP-CPMD method is very promising. They are also quite challenging for two principal reasons. First, they have been done for a density range where calculations indicate the

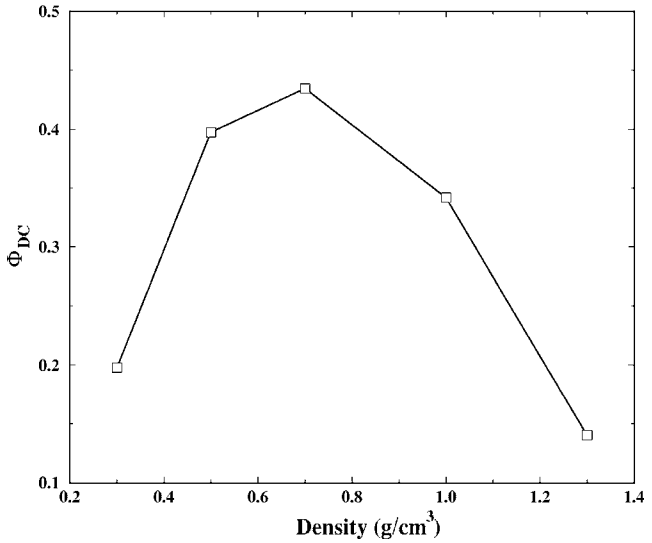

FIG. 4. Dimensionless measure of the fluctuations of the dc conductivity Φ_{dc} of aluminum at $T=10\,000$ K and $\rho=0.3$, 0.5, 0.7, 1.0, and 1.3 g/cm^3 obtained by combining the SCAALP (Ref. 4) and the CPMD (Ref. 17) models.

TABLE III. Values of $\mathcal{S}=2mV_b/\pi e^2 N_e \int_0^\infty d\omega\sigma(\omega)$ averaged over ten configurations of the CPMD calculations for aluminum at $T=10\,000$ K. ρ is the mass density. Integrals in energy have been calculated between 0 and 20 eV.

ρ (g/cm^3)	$\mathcal{S}$
0.01	0.976
0.025	0.983
0.05	0.979
0.1	0.972
0.2	0.972
0.3	0.975
0.5	0.978
0.7	0.985
1.0	0.995

gradual disappearance, with decreasing density, of the Drude behavior. We should expect a reemergence of the Drude behavior of the optical conductivity with decreasing density.[18] The SCAALP model predicts a reincrease of the average ionization below $\rho=0.01$ g/cm^3. This indicates the density range where the reemergence of the Drude behavior should occur with the SCAALP-CPMD method at $T=10\,000$ K. Unfortunately, we could not estimate anything below $\rho=0.01$ g/cm^3 keeping a sufficient number of atoms and good statistics. We could thus not observe any Drude-like reemergence near zero frequency for computational limitation at $T=10\,000$ K. Second, we encountered at intermediate density (i.e., around 0.3 g/cm^3) a significant degree of electronic charge localization which, as already stated before, can be understood by assuming the localization of the atomic $3s$ and $3p$ orbitals. This phenomenon is often delicate to describe with a NPA approach of the type of SCAALP. Indeed, we have seen in Fig. 1 that the SCAALP-CPMD method can noticeably correct the SCAALP predictions for the dc conductivity.

To provide a corroboration to this point, we plot in Fig. 3 the dc conductivity at fixed density $\rho=0.3$ g/cm^3 for various temperatures in the WDM regime. The parameters of the CPMD calculations and the effective HS packing-fractions η_{eff} predicted by the SCAALP model can be found in Table II. Following Desjarlais *et al.*,[18] we have taken only 32 atoms per supercell in order to consider high temperature with a manageable number of excited states. We compare results obtained by the SCAALP model and the SCAALP-CPMD approach to dc conductivity measurements using aluminum

TABLE IV. Values of $\mathcal{S}=2mV_b/\pi e^2 N_e \int_0^\infty d\omega\sigma(\omega)$ averaged over ten configurations of the CPMD calculations for aluminum at $\rho=0.3$ g/cm^3. Temperature T is in kelvin. Integrals in energy have been calculated between 0 and 20 eV.

T (K)	$\mathcal{S}$
10 000	0.988
18 000	0.998
25 000	0.999

foil strips tamped by polished glass plates and rapidly heated by means of a pulse current,[41] exploded wire,[39,40] and an isochoric plasma closed vessel (EPI).[19] Results from the SCAALP model overestimate measurements by a factor of 3. Postprocessing the CPMD code to the SCAALP model is here shown to be crucial, the SCAALP-CPMD results being in excellent agreement with the experimental data.

In Fig. 4, we plot the dimensionless measure of the fluctuations of the dc conductivity Φ_{dc} of aluminum at $T=10\,000$ K for $\rho=0.3$, 0.5, 0.7, 1.0, and 1.3 g/cm^3, respectively. The parameters of the CPMD calculations for 1.0 and 1.3 g/cm^3 are the same (see Table I). For each frequency ω, we calculate the average $\sigma(\omega)$ and the standard deviation $\Delta\sigma(\omega)$ of the optical conductivity over the ten ionic configurations. We then consider the ratio $\Delta\sigma(\omega)/\sigma(\omega)$, which is a dimensionless measure of the fluctuations of the ac conductivity. The dimensionless measure of the fluctuations of the dc conductivity Φ_{dc} is obtained by extrapolating to zero frequency the dimensionless ratio $\Delta\sigma(\omega)/\sigma(\omega)$ using a cubic regression on the points between 0.1 and 1.1 eV. We see that Φ_{dc} as a function of density is maximum around 0.7 g/cm^3. This feature is very interesting because this point is close to the critical point,[22,41] i.e., $\rho\sim 0.7-0.8$ g/cm^3 and $T\sim 6000-8000$ K. It is well known that the amplitude of the fluctuations of many physical quantities become very large near the critical point, until these amplitudes diverge precisely at the critical point.[46] In Fig. 4, we can see an illustration of the importance of the fluctuations of the electrical conductivity near a metal-insulator transition.

Optical constants of material media verify various sum rules.[47–49] The best known is the "f-sum rule" for the optical conductivity $\sigma(\omega)$

$$\mathcal{S}=\frac{2mV_b}{\pi e^2 N_e}\int_0^\infty d\omega\sigma(\omega)=1 \tag{20}$$

that can be obtained as a generalization of the sum rule of the oscillator strength.[50,51] Equation (20) constitutes an important and useful check on the consistency of the optical conductivity. In actual calculations, $\mathcal{S}$ is expected to be smaller than 1, since only a finite, limited number of excited states can be taken into account in the evaluation of Eq. (20). In Tables III and IV, the values of $\mathcal{S}$ corresponding to the cases presented, respectively, in Tables I and II are shown. We note that the identity $\mathcal{S}=1$ is satisfied to better than 3%. In general, the low-frequency part of $\sigma(\omega)$ converges with increasing number of bands much faster than the high-frequency tail, the dc conductivity converges well before the sum rule.[18] The results of Tables III and IV indicate that our values of the dc conductivity are converged to an even higher degree. This explains why no significant differences were observed previously by increasing the number of bands.

IV. CONCLUSIONS

An average-atom model has been coupled to a quantum molecular dynamics code to estimate the optical properties of warm expanded aluminum. Ion configurations are generated using a least-square fit of the pair distribution function deduced from the SCAALP calculations. The optical conductivity of the system is computed from the Kubo-Greenwood formula implemented in the CPMD code. Comparisons between theoretical and experimental results are good. We have shown that the SCAALP-CPMD approach provides an efficient and fast way to compute the optical properties of warm dense aluminum.

ACKNOWLEDGMENTS

We thank M. P. Desjarlais, L. Gremillet, S. L. Libby, R. M. More, and M. S. Murillo for helpful discussions. We are indebted to A. D. Rakhel for sending us the measurement data published in Ref. 41.

*Corresponding author. Email address: gerald.faussurier@cea.fr

[1] J. F. Benage, Phys. Plasmas **7**, 2040 (2000).
[2] R. W. Lee, H. A. Baldis, R. C. Cauble, O. L. Landen, J. S. Wark, A. Ng, S. J. Rose, C. Lewis, D. Riley, J.-C. Gauthier, and P. Audebert, Laser Part. Beams **20**, 527 (2002).
[3] F. Perrot and M. W. C. Dharma-wardana, Phys. Rev. E **52**, 5352 (1995).
[4] C. Blancard and G. Faussurier, Phys. Rev. E **69**, 016409 (2004).
[5] H. Minoo, C. Deutsch, and J. P. Hansen, Phys. Rev. A **14**, 840 (1976).
[6] H. Minoo, C. Deutsch, and J. P. Hansen, J. Phys. (Paris), Lett. **38**, L191 (1977).
[7] F. Perrot and M. W. C. Dharma-wardana, Phys. Rev. A **36**, 238 (1987).
[8] N. W. Ashcroft and N. D. Mermin, *Solid State Physics* (Saunders, Philadelphia, 1976).
[9] R. Car and M. Parrinello, Phys. Rev. Lett. **55**, 2471 (1985).
[10] M. C. Payne, J. D. Joannopoulos, D. C. Allan, M. P. Teter, and D. H. Vanderbilt, Phys. Rev. Lett. **56**, 2656 (1986).
[11] G. Kresse and J. Hafner, Phys. Rev. B **47**, R558 (1993).
[12] A. Alavi, J. Kohanoff, M. Parrinello, and D. Frenkel, Phys. Rev. Lett. **73**, 2599 (1994).
[13] R. Kubo, J. Phys. Soc. Jpn. **12**, 570 (1957).
[14] D. A. Greenwood, Proc. Phys. Soc. London **715**, 585 (1958).
[15] W. A. Harrison, *Solid State Theory* (Dover, New York, 1979).
[16] G. Galli, R. M. Martin, R. Car, and M. Parrinello, Phys. Rev. Lett. **63**, 988 (1989).
[17] P. L. Silvestrelli, Phys. Rev. B **60**, 16382 (1999) and references therein.
[18] M. P. Desjarlais, J. D. Kress, and L. A. Collins, Phys. Rev. E **66**, 025401(R) (2002).
[19] V. Recoules, J. Clérouin, P. Renaudin, P. Noiret, and G. Zérah, J. Phys. A **36**, 6033 (2003).
[20] S. Mazevet, M. P. Desjarlais, L. A. Collins, J. D. Kress, and N. H.

Magee, Phys. Rev. E **71**, 016409 (2005).
[21] P. Renaudin, C. Blancard, G. Faussurier, and P. Noiret, Phys. Rev. Lett. **88**, 215001 (2002).
[22] P. Renaudin, C. Blancard, J. Clérouin, G. Faussurier, P. Noiret, and V. Recoules, Phys. Rev. Lett. **91**, 075002 (2003).
[23] C. Blancard, M. P. Desjarlais, G. Faussurier, V. Recoules, and P. Renaudin, *Proceedings of the 12th APS Topical Conference on Atomic Processes in Plasmas*, edited by S. Mazevet (AIP, College Park, MD, 2004).
[24] D. Marx and J. Hutter, *Modern Methods and Algorithms in Quantum Chemistry*, vol. 1, p. 301 (Forschungzentrum Juelich, NIC Series, 2000).
[25] The CPMD code has been developed by J. Hutter *et al.*, at MPI für Festkörperforschung and IBM Research Laboratory, see also: http://www.cpmd.org
[26] N. D. Mermin, Phys. Rev. **137**, A1441 (1965).
[27] J. Clérouin, P. Renaudin, Y. Laudernet, P. Noiret, and M. P. Desjarlais, Phys. Rev. B **71**, 064203 (2005).
[28] V. Recoules and J.-P. Crocombette, Phys. Rev. B **72**, 104202 (2005).
[29] J.-P. Hansen and I. R. McDonald, *Theory of Simple Liquids*, 2nd ed. (Academic Press, London, 1986).
[30] G. Faussurier and M. S. Murillo, Phys. Rev. E **67**, 046404 (2003) and references therein.
[31] H. Iyetomi and S. Ichimaru, Phys. Rev. A **34**, 433 (1986).
[32] R. G. Gordon and Y. S. Kim, J. Chem. Phys. **56**, 3122 (1972).
[33] R. Evans, B. L. Gyoffry, N. Szabo, and J. M. Ziman, in *The Properties of Liquid Metals*, edited by S. Takeuchi (Wiley, New York, 1973).
[34] R. M. More, Adv. At. Mol. Phys. **21**, 305 (1985).
[35] M. P. Allen and D. J. Tildesley, *Computer Simulations of Liquids* (Oxford University Press, Oxford, 2001).
[36] W. H. Press, S. A. Teukolski, W. T. Vetterling, and B. P. Flannery, *Numerical Recipes in Fortran: The Art of Scientific Computing*, 2nd ed. (Cambridge University Press, New York, 1992).
[37] N. Troullier and J. L. Martins, Phys. Rev. B **43**, 1993 (1991).
[38] P. E. Blöchl and M. Parrinello, Phys. Rev. B **45**, 9413 (1992).
[39] A. W. DeSilva and J. D. Katsouros, Phys. Rev. E **57**, 5945 (1998).
[40] I. Krisch and H. J. Kunze, Phys. Rev. E **58**, 6557 (1998).
[41] V. N. Korobenko, A. D. Rakhel, A. I. Savvatimski, and V. E. Fortov, Phys. Rev. B **71**, 014208 (2005).
[42] G. Röpke, Phys. Rev. A **38**, 3001 (1988).
[43] SESAME: The Los Alamos National Laboratory Equation of State Database, Report No. LA-UR-92-3407, edited by S. P. Lyon and J. Johnson, Group T-1.
[44] F. Perrot, M. W. C. Dharma-Wardana, and J. Benage, Phys. Rev. E **65**, 046414 (2002).
[45] NIST atomic spectra database: http://physics.nist.gov/cgi_bin/AtData/main-asd
[46] J. J. Binney, N. J. Dowrick, A. J. Fisher, and M. E. J. Newman, *The Theory of Critical Phenomena: An Introduction to the Renormalization Group* (Oxford University Press, Oxford, 1992).
[47] M. Altarelli, D. L. Dexter, H. M. Nussenzveig, and D. Y. Smith, Phys. Rev. B **6**, 4502 (1972).
[48] M. Altarelli and D. Y. Smith, Phys. Rev. B **9**, 1290 (1974).
[49] J. D. Jackson, *Classical Electrodynamics* (Wiley, New York, 1999).
[50] G. D. Mahan, *Many-Particle Physics*, 2nd ed. (Plenum Press, New York, 1990).
[51] R. Kubo, M. Toda, and N. Hashitsume, *Many-Particle Physics*, 2nd ed. (Springer Verlag, Berlin, 1995).